# Room temperature AlGaAs/GaAs quantum cascade lasers

Kamil Kosiel*, Anna Szerling, Piotr Karbownik, Iwona Sankowska, Emilia Pruszyńska-Karbownik, Kamil Pierściński, Dorota Pierścińska, Piotr Gutowski, Maciej Bugajski

*Institute of Electron Technology, Al. Lotników 32/46, 02-668 Warszawa*

Received May 10, 2011; accepted June 10, 2011; published June 30, 2011

**Abstract**—The room temperature (293K), pulsed mode operation of a GaAs-based quantum cascade laser (QCL) is reported. This has been achieved by the use of GaAs/$Al_{0.45}Ga_{0.55}As$ heterostructure. Its design follows an "anticrossed-diagonal" scheme. The QCL structures were grown by MBE in a Riber Compact 21T reactor. The double trench lasers were fabricated using standard processing technology, i.e., wet etching and $Si_3N_4$ for electrical insulation. Double plasmon confinement with Al-free waveguide has been used to minimize absorption losses. High operating temperatures have been achieved by careful optimization of growth technology and using metallic high reflectivity facet coating on the back facet of the laser.

In the recent years, quantum cascade lasers (QCLs) have experienced tremendous progress in terms of output power and efficiency. Nevertheless, the performance of GaAs-based QCLs is still inferior to InP devices and room temperature operation is difficult to achieve [1-3]. This is in part due to high threshold current densities (~15kA/cm$^2$ at RT) producing a very high heat load in the devices, even under pulsed operating conditions [4].

The laser structures studied in this paper consisted of the 36-period sequence of injector+3QW segments made of $Al_{0.45}Ga_{0.55}As$/GaAs-coupled quantum wells. The active region was based upon the three quantum well design. The layer sequence of one period of the structure, in nanometers, from left to right, starting from the injection barrier is: **4.6**, 1.9, **1.1**, 5.4, **1.1**, 4.8, **2.8**, 3.4, **1.7**, 3.0, **1.8**, 2.8, **2.0**, 3.0, **2.6**, 3.0 nm. AlGaAs layers are denoted in bold. The total thickness of one period is 45.0 nm. The underlined layers are *n* doped to preserve charge neutrality of the structure and to prevent formation of high field domains under the applied bias. The injector doping was ~ 2.2x10$^{12}$cm$^{-2}$ per period. Only two barrier–QW pairs in the central part of each injector have been doped. The structure used a double-plasmon Al-free waveguide for planar optical confinement.

The core of the structure was embedded in the lightly doped waveguide composed of 3.5μm thick n-GaAs layers on each side (n=4.0x10$^{16}$cm$^{-3}$) terminated by 1μm thick highly Si doped (n=1.0x10$^{19}$cm$^{-3}$) GaAs layers. The details of the technology are given in earlier papers [5-7].

The electronic band structure of QCL, calculated by solving the Schrödinger equation with position dependent effective mass is shown in Fig.1. The calculated transition energies are relatively insensitive to small thickness variations of individual layers, providing the period length is kept within ±2%. The devices with even larger deviation of the period length were still lasing, however, at substantially different wavelength and with lower power.

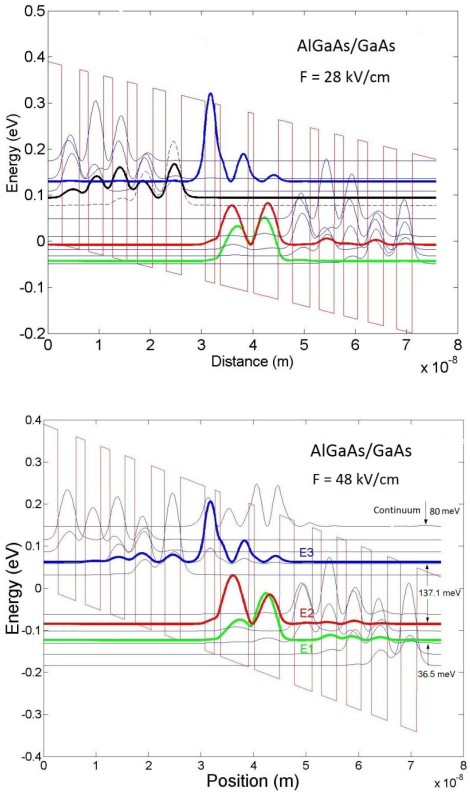


Fig. 1. Conduction band profile and moduli squared wavefunctions in injector/active/injector segment of the laser under an applied field F=28kV/cm (below threshold) and F=48kV/cm (at threshold). The wavefunctions have been shifted to the energy positions of the respective levels. The E3, E2 and E1 refer to the upper, lower and ground state of lasing transitions. The thin blue lines are the injector miniband states. The lowest energy state in the injector couples directly to the upper laser level E3. The topmost state is the Γ continuum state.

In this paper we aimed at the reduction of mirror losses by applying high reflectivity metallic coating. As a result, room temperature operation has been achieved.

* E-mail: kosiel@ite.waw.pl

 

The laser structures were grown by solid source MBE in a Riber Compact 21T reactor. The beams of group III elements were generated by standard effusion cells. The beam of $As_4$ molecules was produced by the valved-cracker as an effusion cell. The substrate temperature was kept at $580^0$C. The value of the V/III BEP ratio was at least 35 for the growth of both GaAs and $Al_{0.45}Ga_{0.55}As$ layers.

In order to adjust highly controllable and optimum growth conditions, the multi-step interrupted growth processes were performed. Additional MBE system calibrations were carried out during the designed growth interruptions. This approach was combined with the relatively low growth rate of active core layers, in order to suppress the negative effects of elemental flux instabilities.

For obtaining information about the thickness and composition of component layers of QCL structure, double-crystal rocking curve measurements were carried out. The dynamical diffraction theory has been used for simulating the symmetric (004) and (002) reflections, leading to the extraction of structural parameters of periodic structures. A detailed analysis of measured HRXRD rocking curves yields the period length equal to 45.1 nm, whereas the intended one was 45.0 nm The barrier layers have been found to contain a smaller amount of Al than intended, i.e. 44%, which is, however, not critical for lasing. The experimental and simulated HRXRD rocking curves are shown in Fig.2.

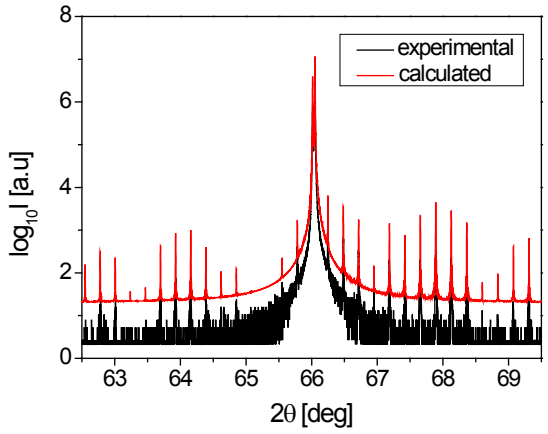


Fig. 2. Comparison of the experimental and simulated HRXRD rocking curves for the QCL structure. The period length and Al content in barriers are determined by a fitting simulated curve to the experimental one.

The double trench lasers were fabricated using standard processing technology, i.e., wet etching and $Si_3N_4$ for electrical insulation. The low resistivity Ni/AuGe/Ni/Au ohmic contacts, alloyed in $430^0$C, were used at the top of the devices. For current injection, windows were opened through the insulator with width 15, 25, and 35μm. After the wafer was thinned down to about 100μm, an alloyed AuGe/Ni/Au contact was deposited on the backside. The lasers were cleaved into bars of 1, 1.5 and 2mm length and the soldered epilayer down on copper submounts [6]. We have used indium soldering or direct Au/Au bonding. Typical device thermal resistance was ~30K/W [8].

In order to reduce mirror losses, we have developed metallic mirror coatings for high reflectivity [9]. The $Al_2O_3/Au/Al_2O_3$ (100nm/100nm/100nm) HR coatings were applied to the back facet of the laser and have shown near 100% reflectivity. Before the coating deposition the laser facet were treated with $Ar^+$ plasma to remove native oxide. The lasers using this technology show improved performance, i.e., reduced threshold $J_{th}$ and increased slope efficiency per facet. In this experiment we have varied mirror losses while waveguide losses can be considered unchanged. The threshold current reduction is then given by the formula:

$$\gamma = \frac{\alpha_i + \alpha_{m,unc}}{\alpha_i + \alpha_{m,c}} = \frac{\alpha_i + \frac{1}{L}\ln\frac{1}{R}}{\alpha_i + \frac{1}{2L}\ln\frac{1}{R}} \quad (1)$$

where $\alpha_{m,unc}$ and $\alpha_{m,unc}$ are the mirror losses for uncoated and coated facet, respectively. Assuming $\alpha_i$=20cm$^{-1}$, $L$=1.5mm and $R$=0.27 one gets $\gamma$=1.2, which is in agreement with the experiment. Defining slope efficiency as:

$$\eta_e = \eta_i \frac{\alpha_m}{\alpha_m + \alpha_i} \quad (2)$$

we can calculate the expected increase in the slope efficiency due to HR coating of the back laser facet as equal to 1.7 for the considered laser. Figure 3 shows experimental L-I characteristics of the laser with HR coating at different temperatures.

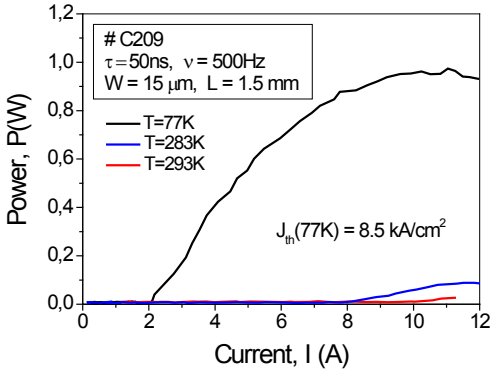


Fig. 3. Light–current characteristics of the laser with HR coatings.

The laser worked up to 293K ($20^0$C), emitting 25mW pulse power. By lowering the laser temperature to $10^0$C, the optical power could be increased to 100mW. The slope efficiency was 0.2W/A at 77K and 0.025W/A at room temperature. The wall plug efficiency at 77K was only ~5% due to the high threshold current caused mainly

 

by high internal losses. The waveguide losses estimated by measuring devices with a different resonator length, fabricated from the same epitaxial wafer, are of the order of 30cm$^{-1}$. The threshold current density can be calculated from the equation [6]:

$$J_{th} = \frac{\varepsilon_0 n \lambda L_p \gamma_{32}}{4\pi e \Gamma |z_{32}|^2} \frac{\alpha_w + \alpha_m}{\tau_3 (1 - \tau_{21}/\tau_{32})} \quad (3)$$

where the injection efficiency of unity in the upper laser level E3 is assumed and direct tunnelling processes out of levels E2 and E3 are neglected. In this equation, $\varepsilon_0$ is the vacuum permittivity, $n$ is the effective refractive index of the laser mode, $\lambda$ is the emission wavelength, $L_p$ is the length of one segment, $\gamma_{32}$ is the full width at the half maximum (FWHM) of the spontaneous emission spectrum, $e$ is the electron charge, $\Gamma$ is the confinement factor and $z_{32}$ is the matrix element of the laser transition. The scattering times $\tau_{ij}$ from states $i$ to $j$ are dominated by LO-phonon emission [7]. The mirror losses $\alpha_m=\alpha_{m,c}=\ln(R)/2L$, where R=0.27 is the uncoated mirror reflectivity. Taking experimentally determined waveguide losses $\alpha_w$ equal to 30cm$^{-1}$, the confinement factor $\Gamma$=0.27 and the effective refractive index $n$=3.27 [10] as well as $\lambda$=9.5μm, $\tau_{32}$=2.1ps and $\gamma_{32}$=16meV, we get $J_{th}$ for the 1.5-mm-long device equal to ≈7kA/cm$^2$, which is basically what we observe experimentally. The possible reason for high internal losses is not optimized injector doping.

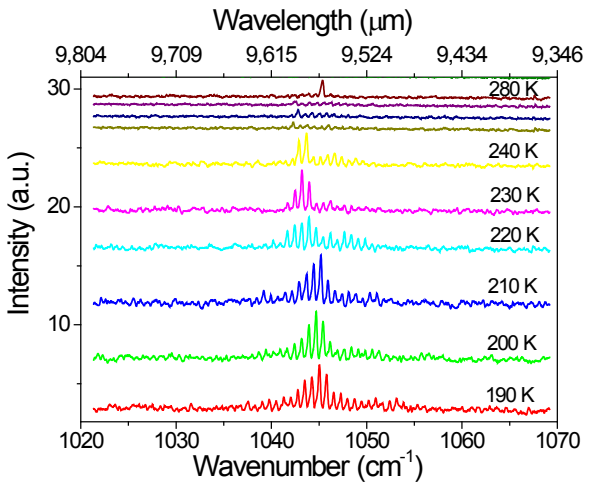


Fig. 4. Optical spectra of Fabry-Perot (FP) laser ($W$=15μm, $L$=1.5mm) at different temperatures for $I$=1.5$I_{th}$.

The Fabry-Perot QC lasers have usually very broad spectra consisting of many longitudinal modes. Figure 4 shows the optical spectra of the device, measured with a Fourier transform infrared spectrometer (FTIR). The spectra exhibit many longitudinal modes with approximately Gaussian envelope. Contrary to standard semiconductor lasers in which carrier diffusion eliminates spatial hole burning, in QCLs the gain recovery process is faster than carrier diffusion, and spatial hole burning is a dominant mechanism, favoring multimode operation [11]. This is mainly due to the unusually fast gain recovery of QCLs, which occurs on a picosecond scale. The lasers with a narrow ridge tend to develop a splitting in the spectrum, approximately equal to twice the Rabi frequency related to the Risken-Nummedal-Graham-Haken instability [12-13].

In conclusion, we have demonstrated room temperature 25mW pulsed operation of an AlGaAs/GaAs mid-infrared (~9.5μm) laser. This has been achieved by careful optimization of the epitaxial process and by applying a high reflectivity metallic coating to the back facet of the laser. Although the measured threshold and efficiency indicate that the devices are not yet fully optimized, the results presented here suggest that the 3QW-AlGaAs/GaAs laser design should be capable of the above room temperature operation.

The work was financially supported by project PBZ-MNiSW 02/I/2007 and project Nr O R00 0053 12.

## References

[1] H. Page, C. Becker, A. Robertson, G. Glastre, V. Ortiz, C. Sirtori, App. Phys. Lett. **78**, 3529 (2001).
[2] H. Page, A. Robertson, C. Sirtori, C. Becker, G. Glastre, J. Nagle, IEEE Phot. Lett. **13**, 556 (2001).
[3] H. Page, P. Collot, A de Rossi, V. Ortiz, C. Sirtori, Semicond. Sci. Technol. **17**, 1312 (2002).
[4] K. Pierściński, D. Pierścińska, K. Kosiel, A. Szerling, M. Bugajski, J. Electronic Mat. **39**, 630 (2010)
[5] K. Kosiel, J. Kubacka-Traczyk, P. Karbownik, A. Szerling, J. Muszalski, M. Bugajski, P. Romanowski, J.Gaca, M. Wójcik, Microelectronics Jour. **40**, 565 (2009).
[6] K. Kosiel, M. Bugajski, A. Szerling, J. Kubacka-Traczyk, P. Karbownik, E. Pruszyńska-Karbownik, J. Muszalski, A. Łaszcz, P. Romanowski, M. Wasiak, W. Nakwaski, I. Makarowa, P. Perlin, Phot. Lett. Poland **1**, 16 (2009).
[7] K. Kosiel, M. Bugajski, A. Szerling, P. Karbownik, J. Kubacka-Traczyk, I. Sankowska, E. Pruszyńska-Karbownik, A. Trajnerowicz, A. Wójcik-Jedlińska, M. Wasiak, D. Pierścińska, K. Pierściński, S. Adhi, T. Ochalski, G. Huyet, *Terahertz and Mid Infrared Radiation* (NATO Science for Peace and Security Series B: Physics and Biophysics, Chapter 13, Springer 2011).
[8] A. Wójcik-Jedlińska, M. Wasiak, A. Szerling, P. Karbownik, K. Kosiel, M. Bugajski, 10th Int. Conf. Mid-infrared Optoelectr. MIOMD, Shanghai, Sept. 5-9, 2010, p.152 (2010).
[9] A. Szerling, P. Karbownik, A. Barańska, K. Kosiel, A. Wójcik-Jedlińska, M. Wasiak, M. Bugajski, 10th Int. Conf. Mid-infrared Optoelectr., MIOMD, Shanghai, Sept. 5-9, 2010, p.156 (2010).
[10] S. Hofling, R. Kallweit, J. Seufert, J. Koeth, J. P. Reithmaier, A. Forchel, J. Crystal Growth **278**, 775 (2005).
[11] A. Gordon, C.Y. Wang, L. Diehl, F. X. Kärtner, A. Belyanin, D. Bour, S. Corzine, G. Höfler, H. C. Liu, H. Schneider, T. Maier, M. Troccoli, J. Faist, F. Capasso, Phys. Rev. A **77**, 053804 (2008).
[12] H. Risken, K. Nummedal, J. Appl. Phys. **39**, 4662 (1968).
[13] P. Graham, H. Haken, Z. Phys. **213**, 420 (1968)

 